Flow visualization of swept wing boundary layer transition

Jacopo Serpieri[1,*] and Marios Kotsonis[1]

[1]Department of Aerodynamics, Wind Energy and Propulsion, Delft University of Technology, Delft, The Netherlands
[*]corresponding author: j.serpieri@tudelft.nl

Abstract In this work the flow visualization of the transition pattern occurring on a swept wing in a subsonic flow is presented. This is done by means of fluorescent oil flow technique and boundary layer hot-wire scans. The experiment was performed at Reynolds number of $2.15 \cdot 10^6$ and at angle of attack of $-3°$. At these conditions, three different flows are investigated: a natural transition case and two other ones where instead the transition mechanism, the stationary cross-flow waves, was forced with discrete roughness elements. Previously published results on similar flows were confirmed for two of the three tested configurations (natural transition and boundary layer forcing at the wavelength of the dominant stationary mode) while, for the third one (where a sub-critical wavelength was forced), some discrepancies are observed. A parametric study on the effect of the Reynolds number and the angle of attack is also presented.
Keywords: 3D subsonic boundary layer transition, Cross-flow stationary waves, Oil flow visualization, Hot-wire.

Nomenclature

Tu	Free stream turbulence
U_∞	Free stream velocity
X	Global axis aligned with the free stream
Y	Global longitudinal axis
Z	Global vertical axis
x	Axis orthogonal to the leading edge
y	Longitudinal axis
y_t	Local wall-normal direction
z	Axis parallel to the leading edge
f	Frequency
c	Chord of the model along X
R	Standard deviation of the surface roughness
Re	Reynolds number based on c and U_∞
α	Angle of attack
f_s	Sampling frequency
f_{co}	Cut-off frequency
λ	Dominant CF wavelength
λ_f	Forced wavelength
d	Roughness elements diameter
k	Roughness elements height
x_{tr}	Transition location along the free stream direction
u	Free stream velocity component
$\bar{u}$	Time-averaged free stream velocity component
HWA	Hotwire anemometry
CF	Crossflow
TS	Tollmien-Schlichting
IR	Infra-red

1 Introduction

The need to investigate the boundary layer transition of three-dimensional flows due to cross-flow *(CF)* instability resides on the fact that this is the main cause of laminar to turbulent transition for swept wing flows in free flight [7]. Experimental campaigns investigating the topic have been pursued by a restricted number of groups around the world on different types of models [1, 6, 5, 2] given the need of having very low turbulence tunnels for this kind of studies. Saric and co-workers [7] showed that the cross-flow instabilities can be of two types depending on the turbulence intensity of the free stream: with a turbulence to free stream velocity ratio such that $\frac{Tu}{U_\infty} < 0.15\%$, standing cross-flow waves (with $f = 0$) were observed, while if the turbulence level is larger, then the scenario is dominated by traveling boundary layer waves. The wave-number vector of both standing and traveling CF waves is approximately perpendicular to the free stream direction. In free flight tests, where the free stream turbulence is usually lower than in wind tunnels experiments, a transition pattern characterized by streaks aligned with the free stream was observed by means of infra-red (IR) thermography [7].

These streaks are the footprint on the wing surface of the stationary cross-flow vortices. The latter are caused by the imbalance between the air particles' kinetic energy and their centripetal acceleration within the boundary layer [1]. Even though the intensity of these instabilities is low compared to the streamwise velocity, they can distort strongly the mean flow field thus being the actual cause of transition to turbulence for the boundary layer flows as the swept wing ones but also the rotating disks or spinning bodies. Mack in 1984 described the stability characteristics of these flows in great detail [4], providing theoretical analysis and experimental data.

Flow visualization can be used to confirm stability characteristics, to prepare an adequate boundary layer quantitative measurement campaign as well as to assess preliminary the flow topology. At the Arizona State University naphthalene sublimation techniques and *IR* thermography were used for the purpose [7].

In the current study, the adopted technique was mineral oil visualization. Results were in fact confirmed with hot-wire *HW* boundary layer scans for several stations along the free-stream direction. The flow evolution was investigated for three different cases: natural transition case, roughness induced instabilities forcing the dominant stationary mode and forcing a sub-critical wavelength. A parametric study on the effect of varying the Reynolds number and the angle of attack on the transition pattern was also carried.

In chapter 2 the experimental apparatus is described. The oil flow visualization is presented in chapter 3.1, while the hot-wire measurements in chapter 3.2. The effect of varying the angle of attack and the Reynolds number is presented in section 3.3.

2 Experimental setup

2.1 Model and wind tunnel

The model chosen for this experiment is a 45 degrees swept wing, with no taper nor twist ratios. A laminar airfoil,resulted from a modification of the NACA 66018, was chosen as the wing section. The choice for such a shape meets the requirements for *CF* investigations illustrated by Bippes [2]: the airfoil needs a favorable pressure gradient where *CF* modes are amplified, it has to have a small leading edge radius to avoid attachment line instability and no concave shape in order to not generate Görtler vortices.

A schematic of the model is presented in figure 1. Two reference systems are showed: a global-windtunnel one defined by upper case symbols (with X aligned with the free stream, Y the horizontal direction and Z the vertical one) and the wing one defined by lower case letters (with x orthogonal to the leading edge line, y coincident with Y and z aligned with the leading edge). The local wall-normal direction is referred as y_t.
The model has a chord in the free stream direction $c \approx 1.3m$ and was installed in LTT wind tunnel at Delft University of Technology *Aerodynamics* laboratories (a closed loop, low turbulence subsonic wind tunnel with a $125cm \times 180cm \times 260cm$ testing section, height, width and length respectively), spanning the whole test section in height and length. The standard deviation of the surface roughness of the model was measured to be $R \approx 0.1\mu m$. The Reynolds number, considering the free-stream direction, was set to $Re = 2.15 \cdot 10^6$ and the angle of attack to $\alpha = -3^\circ$.

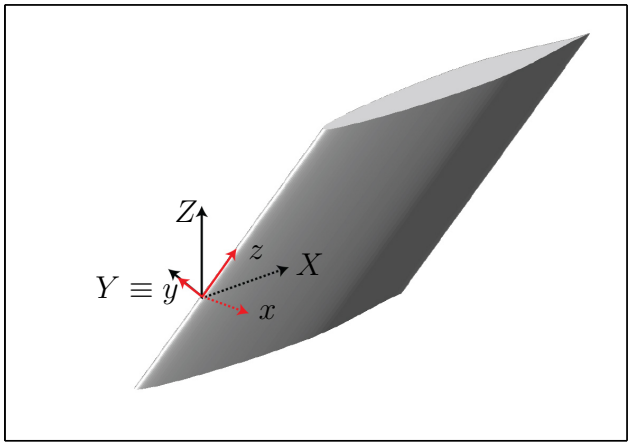

Fig. 1 Wind tunnel reference system XYZ and wing reference system xyz.

2.2 Oil flow visualization

The oil flow techniques is based on a solution of paraffin oil and petroleum with fluorescent pigments dispersed in, for visualization purposes. The solution is painted on the surface model and is then illuminated with an ultra-violet source. Pictures can be captured by normal digital cameras equipped with ultra-violet filters to reduce the reflected light. This oily film is subject to the shear forces the flow exerts on the model and therefore can visualize laminar versus turbulent boundary layers (the latter, exhibiting higher shears then the first, is more effective in tearing the oil away, resulting in darker regions) or other features as flow separation. In this experiment, the oil is meant to visualize the standing *CF* waves. The latter modulating the mean streamwise flow, can be seen as a streaky pattern of the shear stresses. The transition wedges and turbulent breakdown will be captured as well. Particular care was put in painting the model surface with the oil film. The latter need to be the thinnest and most uniform possible in order to reduce the boundary layer contamination.

2.3 Hotwire measurements

For the *HWA* scans, a three degrees of freedom automated traverse was installed in the wind tunnel diffuser. The traverse has a resolution of $2.5\mu m$ in all the three directions. Scans were performed at several stations along the X direction, considering the *(CF)* wave evolution along this direction. This means that the starting Z station at which the scans were performed was not constant but varied while traveling downstream to properly track the waves. Every scan consists of a plane of 3200 points: 50 scans in the local wall-normal direction y_t, to measure the flow evolution within the boundary layer (from the location where the local flow velocity is about the ten percent of the local outer velocity), times 64 locations in the z direction spaced $0.625mm$ from each other. The *HWA* sensor used consisted of a *Dantec P15* boundary layer probe operated by a *TSI IFA-300* constant temperature bridge. Wire calibration was performed in the wind-tunnel itself, far from the model and close to a Pitot probe. Flow temperature correction was also applied in order to account for temperature drifts while running the tunnel. The hotwire was operated at a sampling frequency of $f_s = 50kHz$ and low-pass filtered with a cut-off frequency of $f_{co} = 20kHz$ before bridge amplification. Time-series of 4 seconds were recorded at every probe position to ensure statistical convergence.

3 Results

3.1 Oil flow visualization

Flow visualization in figure 2 shows the flow evolution on the wing suction side from right to left (free stream direction indicated from now on with the light blue arrow). The wing trailing edge is the bright 45 degrees skewed line. The test Reynolds number is $Re = 2.15 \cdot 10^6$, the angle of attack is $\alpha = -3^\circ$ and the transition is naturally occurring (this flow configuration will be referred as *natural transition* case.). Three lines are plotted

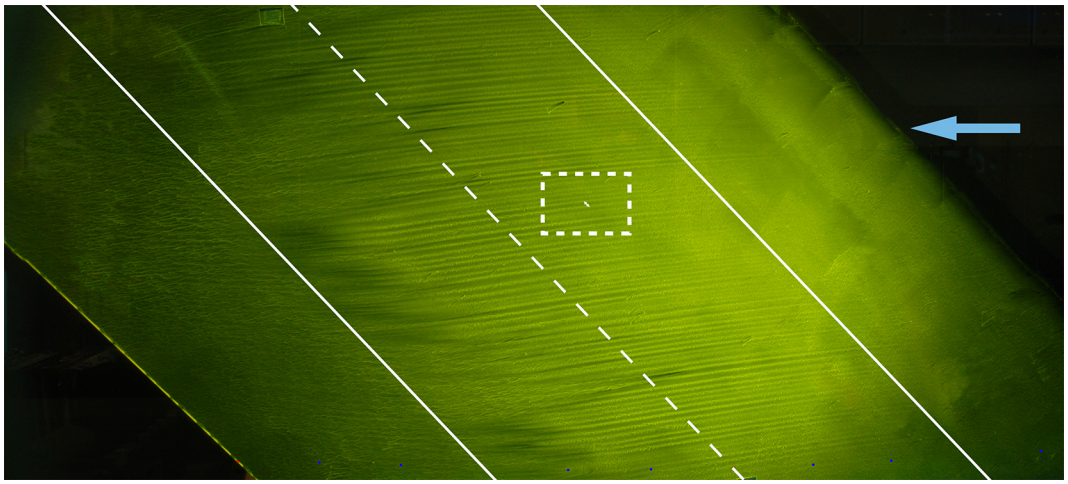

Fig. 2 Fluorescent oil flow visualization on the suction side of the 45° swept wing model installed in the TU Delft LTT wind tunnel at $Re = 2.15 \cdot 10^6$ and $\alpha = -3°$. *Natural transition* case. The white dashed line is the wing mid section $x/c = 0.5$, the other two indicate station $x/c = 0.25$ on the right and station $x/c = 0.75$ on the left respectively.

on top of the picture spaced $0.25c$ from each other: the white dashed line is the wing mid section $x/c = 0.5$, the other two indicate station $x/c = 0.25$ on the right and station $x/c = 0.75$ on the left respectively. This convention will be used throughout the paper. Furthermore in the white dashed box a $10mm$ line is showed as reference. Two regions are distinguishable: the laminar brighter one more on the right and the darker turbulent one that starts unevenly along the span. Several triangular shades with the vertices pointing towards the leading edge are visible, these are the turbulent wedges that indicate the occurrence of turbulence. What can be also clearly seen in the picture are the standing *CF* waves. These consist of a sequence of streaks aligned within few degrees with the free stream flow (the horizontal direction in figure 2). The onset of these streaks as well as their spacing appears irregular along the span. This is related to the occurrence of surface non-uniformities (dust particles, localized roughness, etc...). Besides this, a wavelength of $\lambda \approx 9mm$ is more often observed thus being considered as the dominant standing mode for this flow. In figure 4(a) a detailed view of the white dashed box of figure 2 is presented confirming that the wavelength is of the order of the $10mm$ white line. At the spanwise locations where the streaks first appeared (in a streamwise sense), the transition wedges have their vertices thus clearly indicating that the spatial amplification of the *CF* mode is the transition trigger. Considering a spanwise average, the transition location for this flow can be found occurring around the 65% of the chord. In the aft part of the wing, the occurrence of a turbulent boundary layer deletes the ordered streaks blowing most of the painted oil away.

Radeztsky et al. [5] and Reibert et al. [6] observed that this flow configuration is not the most suitable for boundary layer investigations as it does not provide a spanwise uniform base-flow. As stated before, the flow develops in a very irregular way when comparing different spanwise stations. This because such this flow is very receptive to external disturbances like could be random surface roughness that get stuck on the leading edge region. In order to overcome this condition in their experiment, they decided to impose a more regular base-flow by means of small cylindrical elements (from $6\mu m$ to $36\mu m$ in height and $3-4mm$ of diameter) applied very close to the stagnation line, where the boundary layer results the most receptive. These elements were spaced along the leading edge direction with the characteristic wavelength of the observed standing *CF* wave. In practice they were forcing the most unstable *CF* mode thus leading to a very regular flow pattern characterized by streaks' onset and spacing very well repeated along the span.

In this work the approach of Reibert et al. was followed and a sequence of small cylindrical elements was installed on the model surface close to leading edge of the wing ($x/c = 0.025$). These elements have a diameter of $d = 2.8mm$ and an average height of $k = 10\mu m$. They were installed with a spacing along z of $\lambda_f = 9mm$, this being the wavelength of the dominant standing wave, as showed in figure 5. This configuration is then referred as *critical forcing* case. The consequent flow arrangement is captured in figure 3 for the same Reynolds number and angle of attack considered so far. When comparing this picture to the one of figure 2,

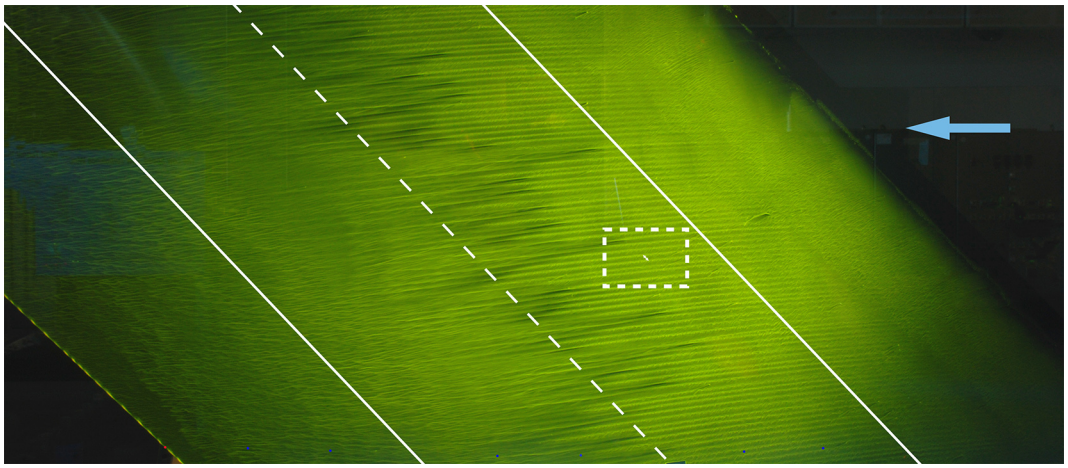

Fig. 3 Fluorescent oil flow visualization on the suction side of the 45° swept wing model installed in the TU Delft LTT wind tunnel at $Re = 2.15 \cdot 10^6$ and $\alpha = -3°$. *Critical forcing* ($\lambda_f = \lambda = 9mm$) case. The white dashed line is the wing mid section $x/c = 0.5$, the other two indicate station $x/c = 0.25$ on the right and station $x/c = 0.75$ on the left respectively.

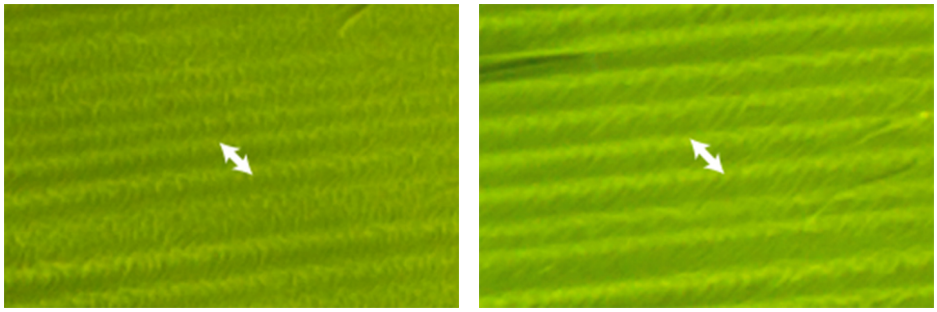

(a) *Natural transition* case (b) *Critical forcing* case.

Fig. 4 Details, corresponding to the white dashed box, of figure 2 and of figure 3. The white reference line is $10mm$ long.

two features appear immediately: the transition front moved considerably towards the leading edge, this is consistent with the findings of Reibert et al. [6] and with the general idea of forcing a naturally unstable mode; the second evident change is the uniformity that the waves of figure 3 present. Forcing the $9mm$ mode in fact led to waves more regularly spaced, with a wavelength equal to the roughness spacing, as it can be observed better in figure 4(b), and with an onset streamwise range considerably narrowed. As a result of this last observation also the transition pattern results more regular and narrowed, with transition wedges less pronounced then in the natural transition case. The average transition location for the $\lambda_f = 9mm$ case is $x/c = 0.45$. With the applied forcing the transition location experienced a shift of about twenty percent of the chord with respect to the *natural transition* case. The small elements ($d = 2.8mm$ and $k \approx 10\mu m$) are capable of strongly enhancing the transition process by deeply modifying the evolution of the standing *CF* waves. The latter result narrowed in the wavelength spectrum by the forcing and augmented in their amplitude thus leading to an anticipated linear saturation and turbulent breakdown [6]. Increasing the dimensions (height and diameter) of the roughness elements was proved by Radeztsky et al. to enhance even further the transition mechanisms and, consequently, anticipating more and more the breakdown location [5].

In the study of Reibert et al. [6], another interesting feature was observed: when the natural wavelength was forced, no higher harmonics were observed in the spanwise scans but instead all the nearest sub-harmonics were present. When they forced a mode with the wavelength three times bigger than the naturally occurring one ($\lambda_f = 36mm$ and $\lambda = 12mm$), they again observed the sub-harmonics, included the natural wavelength, but no super-harmonics.

In this campaign, another flow configuration was tested: the *sub-critical forcing*, with the roughness elements placed with a spacing of $\lambda_f = 5mm$ smaller than the naturally occurring wavelength of $\lambda = 9mm$. It is

to be noted that for this case the same roughness elements ($d = 2.8mm$ and $k \approx 10\mu m$) were used, just their spanwise spacing was modified. The flow picture of this configuration is plotted in figure 6. Again, as for the natural transition case, a wider number of wavelengths can be seen by visually checking the streaks' spacing (see figure 7). The transition region becomes broader in the streamwise extent, with the darker wedges more pronounced. The transition location can be assumed in average occurring at the $x/c = 0.50$ of the model chord.

Table 1 presents a summary of the characteristics of the three configurations investigated. Further insights on the different flow configuration will be gained by the hot-wire scans, the results of which are presented in the next section.

Table 1 Summary of the flow parameters for the investigated cases at $Re = 2.15 \cdot 10^6$ and $\alpha = -3°$.

Case	Forcing	Observed λ	x_{tr}/c
natural transition	none	several	0.65
critical forcing	$9mm$	$9mm$	0.45
sub-critical forcing	$5mm$	$5,9mm$	0.50

3.2 Hot-Wire measurements

In this section the flow configurations, visualized with the fluorescent oil so far, are quantitatively investigated. This is done by means of hot-wire boundary layer scans in planes aligned with the leading edge and the local wall-normal directions (z and y_t respectively) for several streamwise stations (X). As it was anticipated, the starting spanwise location for every scan varied in order to account for the waves' angle with respect to the free stream direction (evaluated in $\approx 5°$ from the oil flow pictures), this achieving a better tracking of the waves' evolution. The time-averaged streamwise velocity component $(\bar{u})$ contours at $x/c = 0.35$, as seen by the flow "entering" the page, for the *natural transition*, for the *critical forcing* and the *sub-critical forcing* cases are presented in figure 8 *a), b)* and *c)* respectively. What appears evident from the figure 8 *a)* is that for the transition process left naturally occurring, the measured waves look very little pronounced. For the *critical forcing* case of figure 8*b*, the waves are much more evident and uniformly spaced along the span (with the same spacing of the roughness elements: $\lambda_f = 9mm$). Reibert et al. [6] measured a similar flow and described these waves as a sequence of co-rotating vortices with the axis oriented within few degrees with the free stream flow. The scenario becomes more complex in figure 8*c*. Here in fact two wavelengths mainly take place: the naturally dominant $\lambda = 9mm$ mode interests the first three waves on the left while the $\lambda_f = 5mm$ mode occurs in the right part of the plane. This picture corresponds to what was plotted in figure 6 where indeed different wavelengths were observable. This preliminary observations, in contrast with the findings of Reibert et al. [6], will need further investigation.

The same contours are now presented at a more downstream location. The planes measured at $x/c = 0.50$ are plotted in figure 9. It has to be noted the different vertical axes of the plots with respect to those of figure 8, to account for the boundary layer growth. The vortices of the *natural transition* case look still very undefined

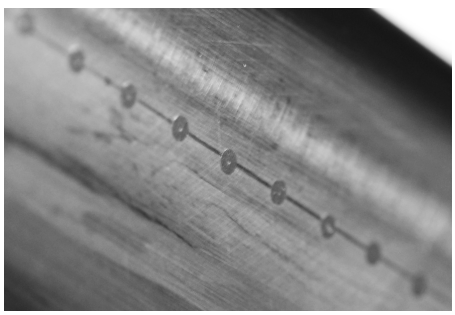

Fig. 5 Cylindrical roughness elements ($d = 2.8mm$ and $k \approx 10\mu m$) installed on the leading edge region ($x/c = 0.025$) of the wind tunnel model with a $9mm$ spacing between consecutive elements.

Fig. 6 Fluorescent oil flow visualization on the suction side of the 45° swept wing model installed in the TU Delft LTT wind tunnel at $Re = 2.15 \cdot 10^6$ and $\alpha = -3°$. *Sub-critical forcing* ($\lambda_f = 5mm$) case. The white dashed line is the wing mid section $x/c = 0.5$, the other two indicate station $x/c = 0.25$ on the right and station $x/c = 0.75$ on the left respectively.

Fig. 7 Detail, corresponding to the white dashed box, of figure 6. The white reference line is $10mm$ long.

apart from the right-end one that largely grew. The $9mm$ waves of figure 9*b* are instead in a more advanced stage: they grew so much that they started falling down on the subsequent one creating more complex structures as the small visible hump at $z \approx 25mm$. As Reibert et al. suggested, at this stage the vortices' linear growth gets saturated thus leaving the floor for modal interactions and secondary high-frequency instabilities [6]. The $\lambda_f = 5mm$ case shows again a more irregular scenario with several modes present. The *critical forcing* case, offering a very uniform base-flow is more suitable for quantitative measurements on *CF* induced transition; the spanwise uniformity allows to assume that the picture showed in figures 8*b* and 9*b* is well repeated also outside the measured domain. Moreover this uniformity is very much needed for comparison with theoretical and numerical studies [3, 7].

At this point, it is interesting to see a larger picture of the flow evolution for the *critical forcing* case and see a comparison between the hot-wire scans and the fluorescent oil visualization. This attempt is presented in figure 10 where a detail of the oil flow visualization, presented in figure 3, is the background for a series of five $\bar{u}$ *HWA* contours for the stations $x/c = 0.15, 0.25, 0.35, 0.50$ and 0.55 of the chord (presented again in figure 11 in a clearer way). The evolution of the waves can then be tracked from a very early stage at $x/c = 0.15$, where they are not yet clearly formed, till their breakdown occurred at $x/c = 0.55$ and passing from the intermediate stations showing the spatial growth they experience ($x/c = 0.35$ already seen in figure 8*b* and $x/c = 0.50$ in figure 9*b*). The underlying oil film shows a good qualitative match with what the boundary layer measurements describe thus being validated as a helpful tool for this type of investigations. It should be noted in fact that in order to obtain the *HWA* scans presented in figure 10, several days are spent running the wind-tunnel with the obvious costs that this requires. Having the chance of qualitatively describing the boundary layer evolution

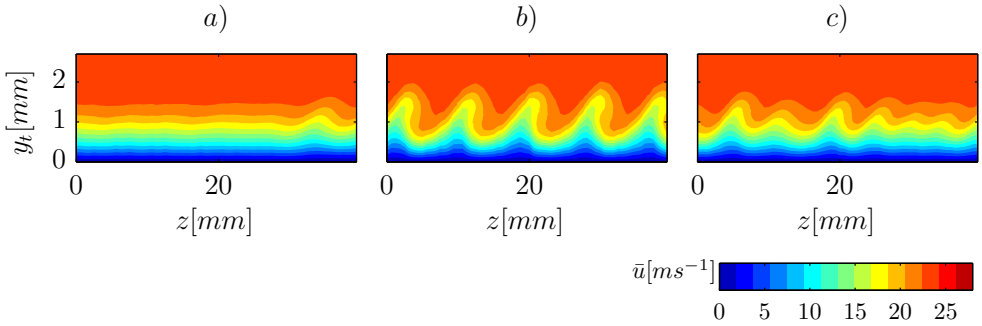

Fig. 8 Contours of the mean streamwise velocity component $\bar{u}$ at $x/c = 0.35$ for $Re = 2.15 \cdot 10^6$ and $\alpha = -3°$. a: *natural transition* case; b: *critical forcing* case; c: *sub-critical forcing* case.

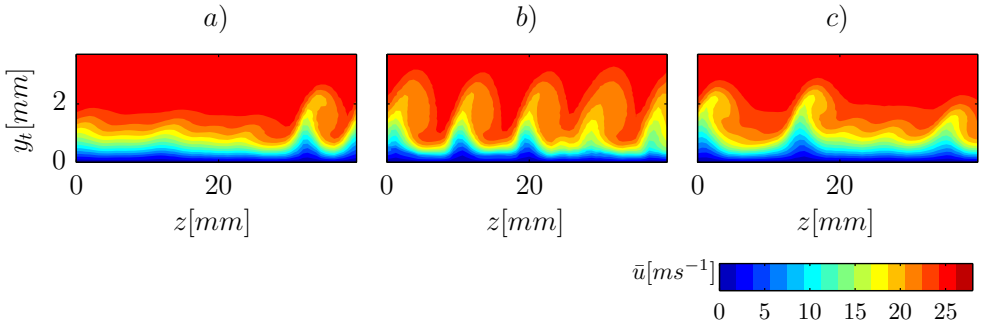

Fig. 9 Contours of the mean streamwise velocity component $\bar{u}$ at $x/c = 0.50$ for $Re = 2.15 \cdot 10^6$ and $\alpha = -3°$. a: *natural transition* case; b: *critical forcing* case; c: *sub-critical forcing* case.

with a single picture is of great relevance.

3.3 Effect of varying α and *Re* on the transition pattern

In this section some other flow cases are presented in order to show the effect of varying α and *Re* on the transition pattern. For all the cases presented here, natural transition is occurring: no roughness elements are installed on the model surface. Furthermore in all the pictures the same reference lines, introduced in section 3.1, are plotted. Moreover the portion of the figures included in the white dashed rectangles are presented apart in detail.

In figure 12(a), the oil flow visualization of the case at $\alpha = -3°$ and $Re = 2.12 \cdot 10^6$ is showed. This flow is similar to what was presented in figure 2 given the same angle of attack and the very close Reynolds number ($Re = 2.15 \cdot 10^6$ in figure 2). Although some features might differ as the spanwise location of the transition

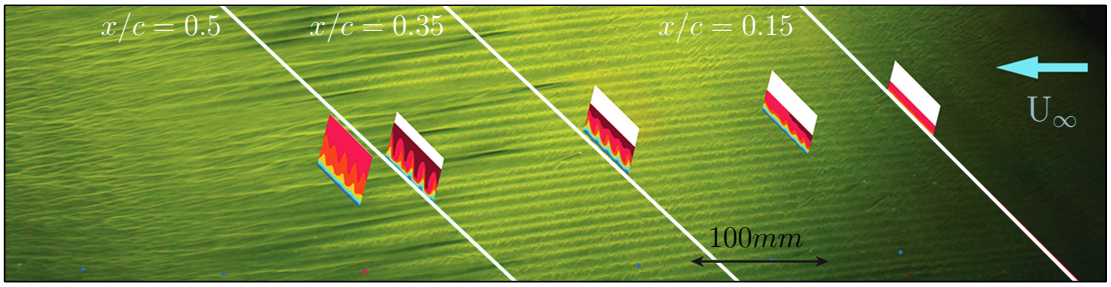

Fig. 10 Contours of the mean streamwise velocity component $\bar{u}$ at several stations ($x/c = 0.15$, 0.25, 0.35, 0.50 and 0.55) superimposed to the oil flow visualization for $Re = 2.15 \cdot 10^6$ and $\alpha = -3°$ for critical forcing ($\lambda_f = \lambda = 9mm$).

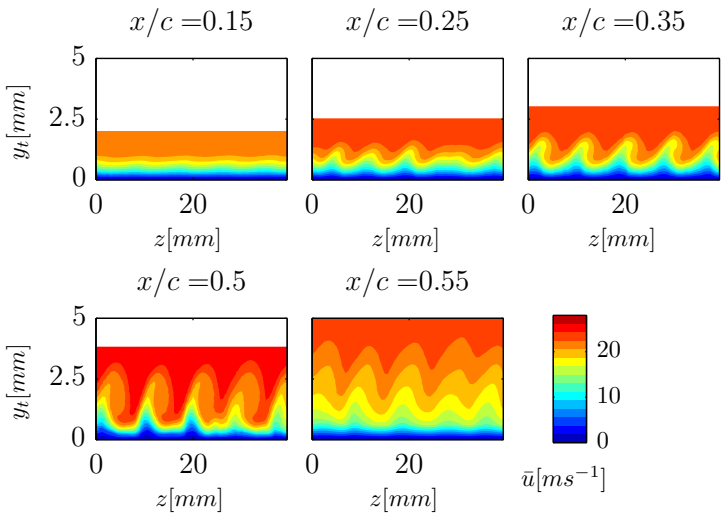

Fig. 11 Contours of the mean streamwise velocity component $\bar{u}$ for the stations $x/c = 0.15$, 0.25, 0.35, 0.50 and 0.55 at $Re = 2.15 \cdot 10^6$ and $\alpha = -3°$. *Critical forcing* case.

wedges. As it was stated before, these flows, where natural transition occurs, are not very robust to little changes in the experimental conditions thus causing the observed discrepancies. Despite this, the spanwise average transition location is again located at $x/c \approx 0.65$; the spacing of the waves is again of the order of $\lambda = 9mm$ as seen in section 3.1.

Changing the angle of attack but keeping constant the free stream velocity, the flow is very much modified. What happens if the angle of attack is increased, is that the favorable pressure gradient is reduced. The cross-flow waves amplification is in fact dependent on the pressure gradient: opposite to Tollmien-Schilichting (*TS*) waves which amplify in positive pressure gradient regions, the cross-flow ones grow in the favorable pressure gradient flows. This explains the choice of a laminar airfoil as the NACA 66018 as the base shape for the test model: its shape is optimized to delay transition caused by *TS* instabilities, by shifting the maximum thickness point towards the trailing edge. As the goal of this study is to study the transition process when *CF* vortices dominate, having an extended region of flow acceleration helps detecting these instabilities [7]. In figure 12(b), the wing was set at $\alpha = 0°$. The streaks became almost invisible, just some very vague shades are distinguishable close to the $x/c = 0.75$ line. Moreover due to the reduced strength of the *CF* modes, no turbulent breakdown occurs and the boundary undergoes laminar separation, followed by turbulent re-attachment more downstream. The separation location is evidenced by the brighter line followed by a darker region.

Changing the free stream velocity, with keeping the angle of attack equal to $-3°$, leads to the results presented in figures 12(a), 13(a) and 13(b). What appears evident is that the flow transition is enhanced by the Reynolds number, as expected [5]. For the case of $Re = 1.7 \cdot 10^6$, the cross-flow instability is still too weak to cause transition. The latter gets delayed till $x/c \approx 0.78$, after the pressure minimum location, thus leading to the amplification of *TS* waves too. It is likely that complicated interactions between the modes of the two different types take place at this location. What is also to be noted by the comparison of the three flows, is that increasing the Reynolds number, it decreases the wavelength of the *CF* waves. Within the $10mm$ reference length, the $Re = 1.7 \cdot 10^6$ case shows approximately one wave (see figure 14(a)), while the $Re = 2.55 \cdot 10^6$ flow, two (see figure 14(b)); the $Re = 2.12 \cdot 10^6$ case being half way from the other two ones. This behavior was already observed by Radeztsky et al. [5] and is here confirmed.

The concluding message of the section is that from qualitative visualization and quantitative measurements the most suiting case for *CF* instability investigation is the one showed in figure 3. The spanwise uniformity is here a key feature while the combination of the angle of attack and Reynolds number is optimal for the amplification of the cross-flow stationary waves leading to turbulent breakdown and transition.

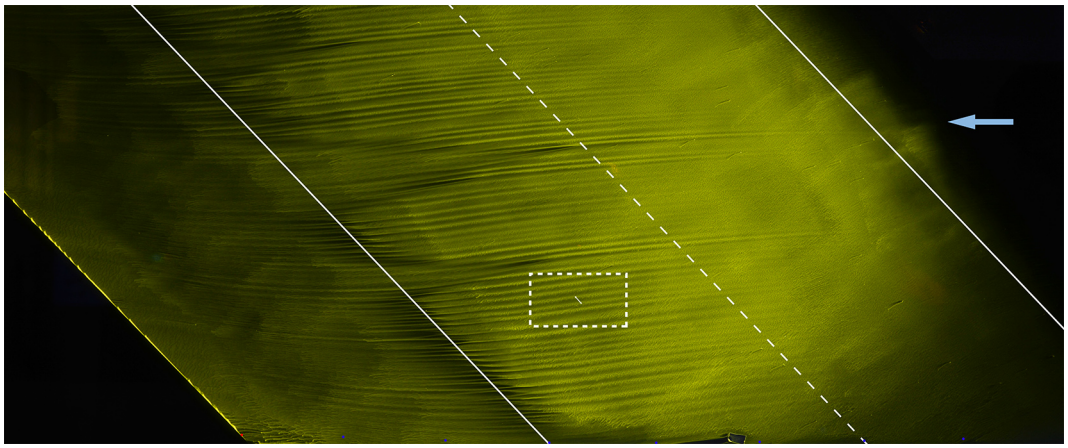

(a) $\alpha = -3°$.

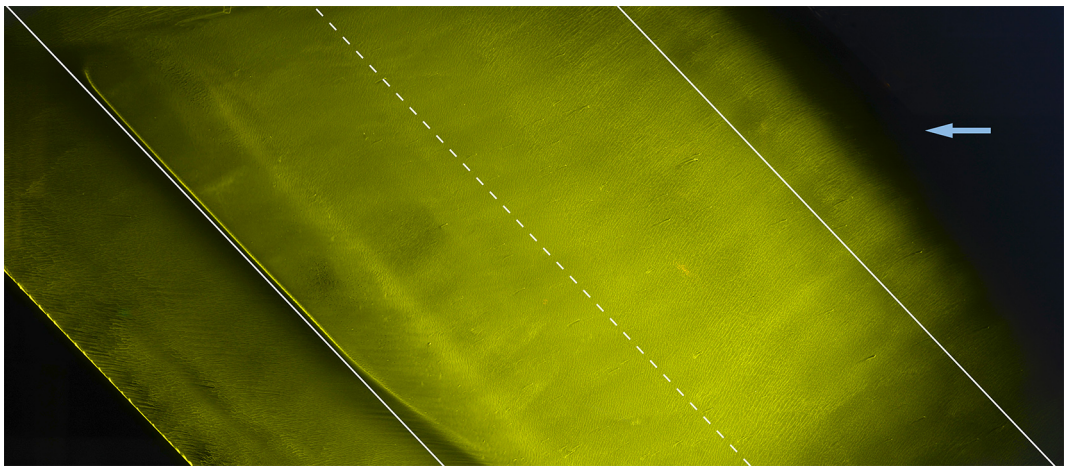

(b) $\alpha = 0°$.

Fig. 12 Flow arrangement varying the angle of attack at $Re = 2.12 \cdot 10^6$.

4 Conclusions

In this work the boundary layer around a 45 degrees swept wing at a Reynolds number of $Re = 2.15 \cdot 10^6$ and an angle of attack of $\alpha = -3°$ is investigated by means of fluorescent oil flow visualization and hot-wire scans. Such a flow, for low values of free-stream turbulence, is characterized by standing waves. These waves, named cross-flow waves, introduce a strong distortion of the mean flow. By spacial amplification, these disturbances grow while moving downstream till the point where the phenomenon is no more linear given the occurrence of modal growth saturation, modes interaction and secondary high-frequency instabilities. The generation and growth of these waves is then the primary cause of transition to turbulence in this type of flows.

The experimental techniques, used so far in literature, encompassed hot-wire and hot-film sensors for quantitative measurements and infra-red thermography and naphthalene sublimation for qualitative description of the flow evolution [7]. From qualitative observations some quantitative information can be extracted though such as the modes' wavelengths, the instability onset and the transition location, this simplifying much the measurements and correctly addressing them.

In this study, the fluorescent oil technique has been successfully deployed and checked comparing its outcome with the hot-wire scans. The use of such this method is not trivial though given the great care it is needed not to contaminate the boundary layer itself. The need of a thin oil film results also from willing be able to observe the flow modulation caused by the standing *CF* waves, in regions where the wall shears are still very low (so not strong enough to efficiently tear away the oil layer).

Three different flow configurations were investigated: the natural transition case and then two cases where

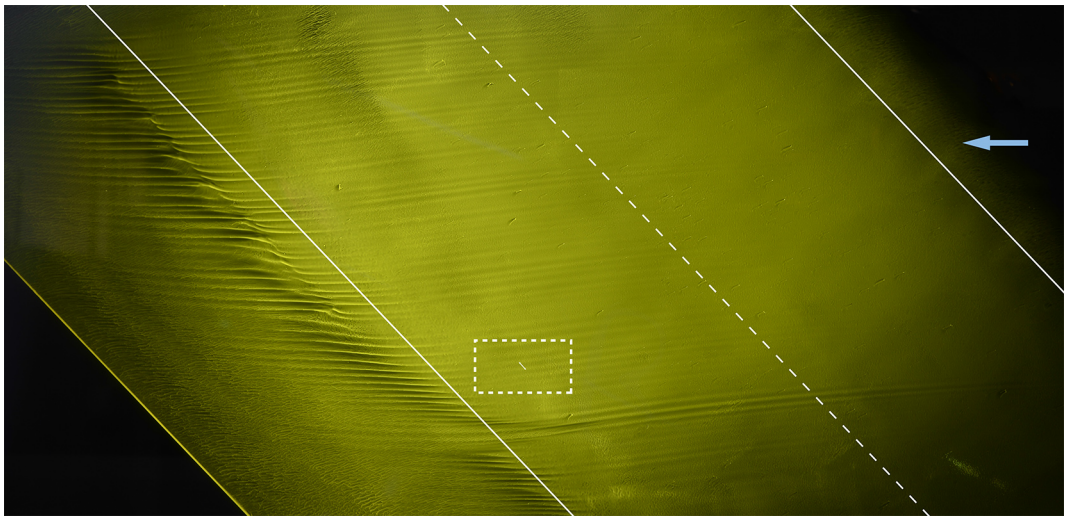

(a) $Re = 1.7 \cdot 10^6$.

(b) $Re = 2.55 \cdot 10^6$.

Fig. 13 Flow arrangement varying the Reynolds number at $\alpha = -3°$.

the cross-flow waves were forced in the boundary layer most receptive region by applying, on the model surface, a series of cylindrical roughness elements (with a diameter of $d = 2.8mm$ and an average height of $k = 10\mu m$) following the works of Reibert et al. and Ratezsky et al. [6, 5]. These elements were spaced accordingly to two configurations: for the *critical forcing* case, at the wavelength of the natural dominant mode and for the *sub-critical forcing* case, they were installed with a smaller in between distance. The flow observed when natural transition occurs, shows several wavelengths and a very late transition location ($x_{tr}/c = 0.65$). Forcing the dominant wavelength leads instead to a very spanwise uniform boundary layer destabilized only by that given mode. Given the initial higher amplitude of this mode, transition results anticipated with respect to the natural transition case, as already observed by Reibert et al. [6], of about twenty percent of the chord ($x_{tr}/c = 0.45$). The third case, with the sub-critical forcing presents aspects from the other two flows: transition is still anticipated but a wider band of modes results amplified in the boundary layer, included larger wavelengths despite previous literature observations [6]. These observations lead the choice of the natural wavelength forcing as the optimal base flow case for quantitative boundary layer measurements given the greater uniformity it shows.

Furthermore the effect of changing the Reynolds number and the angle of attack was visually inspected, leading to results in line with the reported literature [5, 7]. The transition scenario is strongly dependent on these two parameters: increasing (decreasing) the angle of attack effects the pressure distribution on the model thus leading to a smaller (larger) amplification of the stationary cross-flow waves; the Reynolds number also varies the growth rates of these disturbances, as expected, but also effects the natural wavelength: for higher

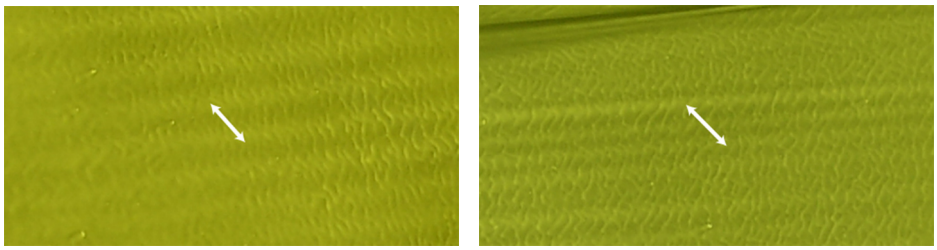

(a) $Re = 1.7 \cdot 10^6$. (b) $Re = 2.55 \cdot 10^6$.

Fig. 14 Details, corresponding to the white dashed box, of figure 13 (a) and (b). The white reference line is 10*mm* long.

Reynolds number, the streaks appear closer to each other.

The flow visualization experiment presented in this study led to a valuable knowledge of the flow evolution, transition pattern and cross-flow waves configuration on the wind tunnel model. This knowledge resulted of fundamental importance for a boundary layer quantitative measurement campaign.

Acknowledgments

The authors express their gratitude to Mr. Leo Molenwijk and Mr. Stefan Bernardy for their valuable assistance in the laboratory. This project is founded by the Netherlands Organisation for Scientific Research *NWO-STW* under the *Veni* grant.

References

[1] Arnal, D., Gasparian, G. and Salinas, H. (1998). Recent advances in theoretical methods for laminar-turbulent transition prediction. *AIAA Journal*, vol. 98-0223.

[2] Bippes, H. (1999) Basic experiments on transition in three-dimensional boundary layers dominated by crossflow instability. *Prog. Aero. Sci.*, vol. 35, pp 363-412.

[3] Haynes, T. S. and Reed, H. L. (2000) Simulation of swept-wing vortices using non-linear parabolized stability equations. *Journal of Fluid Mech.*, vol. 405, pp 325-349.

[4] Mack, L. M. (1984) Boundary-layer linear stability theory. *AGARD Report 709*.

[5] Radeztsky, R. H., Reibert, M. S., Saric, W. S. (1999) Effect of isolated micron-sized roughness on transition in swept-wing flows. *AIAA Journal* vol. 11, pp 1370-1377.

[6] Reibert, M. S., Saric, W. S., Carrillo, R. B., Chapman, K. L., (1996) Experiments in a nonlinear saturation of stationary crossflow vortices in a swept-wing boundary layer. *AIAA Journal* vol. 11, pp 1370-1377.

[7] Saric, W. S. and Reed, H. L. and White, E. B. (2003) Stability and transition of three-dimensional boundary layers. *Annual Review of Fluid Mechanics* vol. 35, pp 413-440.

[8] Saric, W. S., Carpenter, A. L. and Reed, H L. (2011) Passive control of transition in three-dimensional boundary layers, with emphasis on discrete roughness elements. *Phil. Trans. R. Soc.* vol. 369, pp 1352-1364.